Removal of *pomt1* in zebrafish leads to loss of α-dystroglycan glycosylation and dystroglycanopathy phenotypes

Brittany F. Karas[#], Kristin R. Terez[#], Namarata Battula, Brian M. Gural, Kyle P. Flannery, Grace Aboussleman, Numa Mubin, M. Chiara Manzini[*]

Department of Neuroscience and Cell Biology, Child Health Institute of New Jersey, Rutgers University-Robert Wood Johnson Medical School, New Brunswick, NJ 08901 USA.

# these authors contributed equally

***Corresponding Author:**

M. Chiara Manzini

Department of Neuroscience and Cell Biology

Child Health Institute of New Jersey

Rutgers University-Robert Wood Johnson Medical School

New Brunswick, NJ 08901 USA

Phone: 732-235-3245

Email: chiara.manzini@rutgers.edu

Abstract

Biallelic mutations in *Protein O-mannosyltransferase 1* (*POMT1*) are among the most common causes of a severe group of congenital muscular dystrophies (CMDs) known as dystroglycanopathies. POMT1 is a glycosyltransferase responsible for the attachment of a functional glycan mediating interactions between the transmembrane glycoprotein dystroglycan and its binding partners in the extracellular matrix (ECM). Disruptions in these cell-ECM interactions lead to multiple developmental defects causing brain and eye malformations in addition to CMD. Removing *Pomt1* in the mouse leads to early embryonic death due to the essential role of dystroglycan in embryo implantation in rodents. Here, we characterized and validated a model of *pomt1* loss of function in the zebrafish showing that developmental defects found in individuals affected by dystroglycanopathies can be recapitulated in the fish. We also discovered that *pomt1* mRNA provided by the mother in the oocyte supports dystroglycan glycosylation during the first few weeks of development. Muscle disease, retinal synapse formation deficits, and axon guidance defects can only be uncovered during the first week post fertilization by generating knock-out embryos from knock-out mothers. Conversely, maternal *pomt1* from heterozygous mothers was sufficient to sustain muscle, eye, and brain development only leading to detectable muscle disease and loss of photoreceptor synapses at 30 days post fertilization. Our findings show that it is important to define the contribution of maternal mRNA while developing zebrafish models of dystroglycanopathies and that offspring generated from heterozygous and knock-out mothers can be used to differentiate the role of dystroglycan glycosylation in tissue formation and maintenance.

Introduction

Dystroglycanopathies are a group of rare autosomal recessive neuromuscular disorders which include the most severe forms of congenital muscular dystrophy (CMD). These diseases also affect the eye and brain and lead to early mortality (1,2). The primary molecular deficit is the loss of interactions between the extracellular portion of the transmembrane glycoprotein dystroglycan, α-dystroglycan (α-DG), and ligands in the extracellular matrix (ECM) (2). These interactions are mediated via a large, specialized O-linked glycan on α-DG termed matriglycan assembled via multiple glycosyltransferases (2,3). Biallelic mutations in *dystroglycan* (*DAG1*, OMIM:128239) itself have been identified as the cause of primary dystroglycanopathy (OMIM:613818, 616538), but they are exceedingly rare (4). Most cases of dystroglycanopathies are deemed secondary and are caused by variants in the glycosyltransferases involved in catalyzing the synthesis of matriglycan (2).

Protein O-mannosyltransferase 1 (*POMT1*, OMIM:607423) catalyzes the addition of an O-linked mannose to α-DG starting the assembly of the functional glycan (5). *POMT1* mutations are one of the most frequent causes of dystroglycanopathy in multiple populations and lead to the full spectrum of disease from limb-girdle muscular dystrophy (POMT1-LGMD, OMIM:609308) to severe CMD disorders affecting the brain and the eyes such as Walker Warburg Syndrome (WWS) (OMIM:236670) (6–8). Global knock-out (KO) of *Pomt1* in the mouse leads to early embryonic lethality similarly to *Dag1* mutants. This is due to the critical role of dystroglycan in Reichert's membrane, a specialized basement membrane in rodent embryos (9,10). Thus, *Pomt1* mouse models have only been studied using conditional approaches (11,12).

We sought to develop a novel animal model of dystroglycanopathies by characterizing *pomt1* loss of function in the zebrafish. The zebrafish has become an established model for muscle disease because of the molecular and physiological conservation of disease mechanisms, their external embryonic development, and their fecundity accompanied with small size which allows for high-throughput drug screening for motor phenotypes (13,14). Most zebrafish models for dystroglycanopathies to date have been generated via gene knockdown using morpholino oligonucleotides (MOs) to validate genetic findings in humans. The same array of phenotypes including loss of α-DG glycosylation, shortened body axis, reduced mobility, muscular dystrophy, and eye and brain malformation were found in knockdown models of multiple glycosyltransferases (15–19). However, knockdown approaches are limited by their variable and transient effect. Furthermore, results of *pomt1* knockdown in larvae were unexpectedly mild compared to other dystroglycanopathy zebrafish knockdowns (19).

Out of the nineteen dystroglycanopathy genes, there are currently three zebrafish genetic models reported. The *patchytail* mutant was generated via a mutagenesis screen leading to a missense mutation in *dag1* and loss of the protein. These mutants die by 10 days post fertilization and show similar deficits to the morphants, although less severe, which recapitulate multiple aspects of the human presentation in the muscle, eye, and brain (20). KO larvae for the glycosyltransferase *fukutin-related protein* (*fkrp*) more closely phenocopied the morphants and were then used to study the effects of overexpression of the most common *FKRP* (OMIM: 606596) missense variant leading to *FKRP*-related LGMD (OMIM:607155) to identify compounds that could ameliorate motor phenotypes by drug screening (21). Interestingly, no motor or developmental phenotypes were described for zebrafish CRISPR mutants developed for another glycosyltransferase *protein O-mannose β-1,2-N-acetylglucosaminyltransferase* (*pomgnt1*) (22). However, *pomgnt1* KOs showed photoreceptor degeneration in the retina between 2 and 6 months of age, reflecting retinal deficits identified in patients (23). Hypomorphic variants in *POMGNT1* have also been linked with non-syndromic retinitis pigmentosa (24). These studies indicated that relevant phenotypes resulting from global KOs of dystroglycanopathy genes can be successfully modeled in zebrafish. Due to the genetic heterogeneity of dystroglycanopathies, testing zebrafish models for multiple genes will be beneficial to identify compounds that would be effective in individuals with distinct genetic causes.

Here, we show that *pomt1* KO zebrafish show varying degree of muscle, eye, and brain phenotypes depending on whether *pomt1* mRNA is provided to the oocyte from the mother. Since the eggs are externally fertilized, zebrafish females provide nutrients, mRNAs, and proteins to support early development in the yolk (25). *pomt1* KOs obtained from heterozygous mothers can compensate for the early developmental phenotypes by having maternally provided Pomt1 glycosylate α-DG. More severe phenotypes appear when KO embryos are generated by a KO mother. Our work indicates that special consideration must be taken regarding the potential maternal contribution in future dystroglycanopathy mutants.

Results

A late nonsense allele in pomt1 leads to complete protein loss and loss of α-DG glycosylation

In order to determine whether loss of *pomt1* would lead to dystroglycanopathy phenotypes in the zebrafish, we obtained a *pomt1* line generated through a N-ethyl-N-nitrosurea (ENU) mutagenesis screen by the Zebrafish Mutation Project (ZMP line: sa146678, kind gift of Dr. James Dowling, Sick Kids, Toronto, Canada) (**Fig.1A**) (26). This line introduced a variant in exon 19 of *pomt1* (NM_001048067: c.1911T>A) leading to a stop codon (NP_001041532: p.Tyr637Ter) towards the C-terminus of the 720

amino acid protein. Since multiple homozygous nonsense and frameshift variants had been reported in humans to cause the most severe form of dystroglycanopathy, WWS (27,28), we hypothesized that this zebrafish variant could lead to nonsense mediated decay of the mRNA and complete protein loss. We bred the p.Tyr637Ter variant into homozygosity and confirmed the variant by Sanger sequencing (**Fig.1B**). Through quantitative PCR (qPCR) analysis we found that *pomt1* mRNA was reduced in both heterozygous and homozygous fish between 5 and 40 days post fertilization (dpf) with the exception of the 10 dpf timepoint where there was an increase (**Fig.1C**). The Pomt1 protein was completely lost at 30 dpf in homozygous animals and no additional truncated band was noted, apart from a non-specific band which is also present in wild-type (WT) samples (**Fig.1D**). In parallel, we confirmed that Pomt1 function was completely lost. No α-DG glycosylation was found using a glyco-specific antibody in wheat germ agglutinin (WGA) enriched zebrafish head tissue from 30 dpf animals, though β-DG expression was preserved (**Fig.1E**). In summary, the *pomt1*^{Y637X} line leads to complete loss of function of Pomt1 and will be termed as *pomt1* KO.

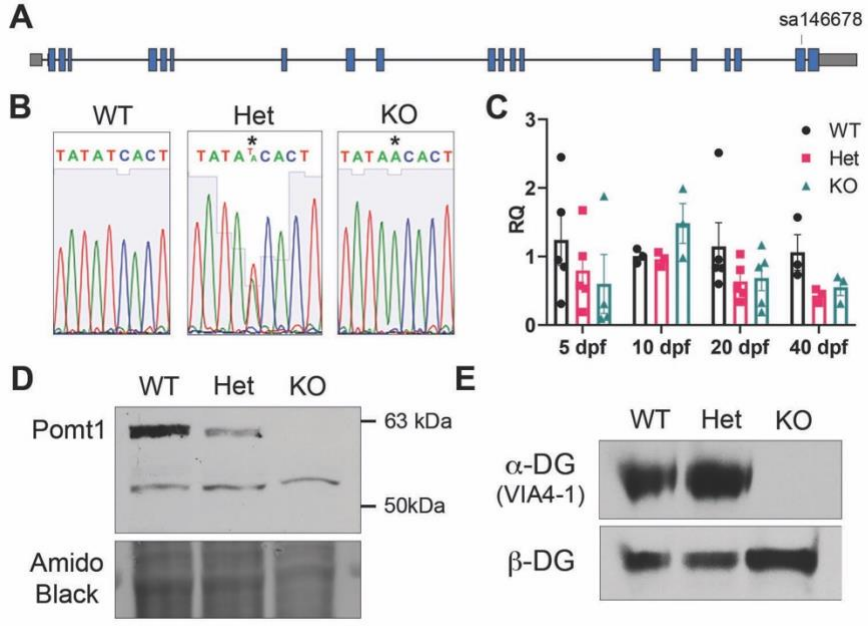

Figure 1. *pomt1* nonsense variant leads to complete loss of protein and protein function. A. Schematic of the gene structure of *pomt1* including the location of the variant in exon 19. **B.** Sanger sequencing validation shows the stop codon generated in the KO genome. **C.** qPCR analysis showed consistent reduction in *pomt1* mRNA apart from 10 dpf. **D.** Pomt1 is completely absent on Western blot in 30 dpf protein lysates. **E.** α-DG glycosylation is absent in KO tissue while β-DG expression is preserved.

Loss of pomt1 from heterozygous crosses leads to reduced survival and muscle disease

No phenotypes had been reported in *pomt1* KO zebrafish larvae by the ZMP. Thus, we performed a comprehensive analysis of *pomt1* KO fish obtained from heterozygous (Het) parents. Survival analysis revealed that *pomt1* KO juveniles start dying between 30 dpf and 40 dpf (30 dpf: WT 24.3±8.0%, n=18; Het 49.0±9.5%, n=41; KO 27.7±2.0%, n=17, N=3 clutches. 40 dpf: WT 28.0±4.0%, n=22, Het 60.3±7.5%, n=46, KO 11.7±3.5%, n=11, N=3 clutches) with no survival observed beyond 70 dpf (**Fig.2A**). While no morphological differences were noted at 5 and 20 dpf, significant differences in body length emerged at 30 dpf (WT 8.5±0.5 mm, n=18; Het 7.3±0.3 mm, n=41; KO 6.2±0.2 mm, n=17; WT-Het p=0.039 *, WT-KO p=0.0005 ***) (**Fig. 2B**). *pomt1* KO juveniles were smaller and showed a delay in development with less prominent dorsal and anal fins (**Fig.2C**). Interestingly, the surviving KO fish at 40 dpf were the largest of that genotype (WT 9.6±0.4 mm, n=22; Het 9.9±0.3 mm, n=46; KO 8.5±0.4 mm, n=11). This finding suggests that smaller KO fish likely died due to the inability to compete for food. As such, only the least affected fish survived.

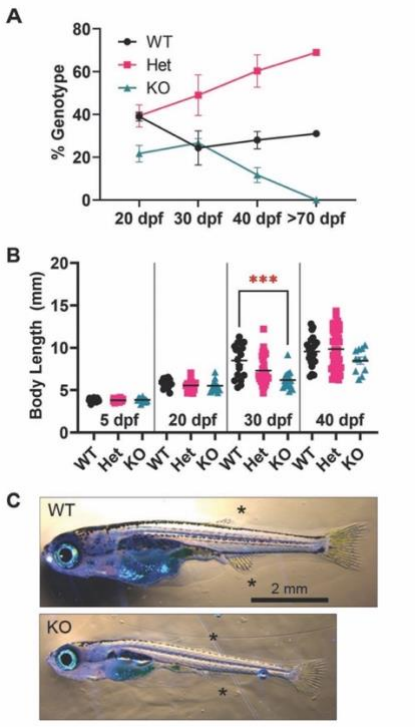

Figure 2. *pomt1* KO fish show reduced survival and size. A. Survival curves show a drop in *pomt1* KO juveniles after 30 dpf. **B.** Significant size differences are evident in KO fish at 30 dpf, but not in the surviving KO fish at 40 dpf. *** p<0.001 **C.** *pomt1* KO fish at 30 dpf appear underdeveloped with less prominent dorsal and anal fins (asterisks). Scale bar: 2mm.

We tested motor function in an automated DanioVision™ tracking system where the fish were allowed to swim freely for 30 minutes. No differences were noted in 5 dpf larvae (**Suppl. Fig. 1A-C**). While only a trend for reduced distance covered and swimming velocity was found in 30 dpf *pomt1* KOs (WT n=15, Het n=37, KO n=13, N=3 clutches. Distance: WT 870.5±84.9 cm, Het 803.9±54.7 cm, KO 666.2±88.9 cm, WT-KO p=0.51. Velocity: WT 0.485±0.047 cm/s, Het 0.449±0.030 cm/s, KO 0.380±0.051 cm/s, WT-KO p=0.62) (**Fig.3A-B**), we found a significant reduction in acceleration when compared to both Het and WT fish (WT 420.1± 24.0 cm/s^2, Het 401.6±23.3 cm/s^2, KO 291.0±27.8 cm/s^2, WT-KO p=0.024 *, Het-KO p=0.018 *) (**Fig. 3C**). Histological analysis of the muscle at 30 dpf was complicated by the extreme fragility of the tissue in KO animals where myofibers tended to fragment. Via hematoxylin-eosin staining in paraffin sections, we found that myofibers where short and separated from each other often with gaps in the myosepta (**Fig.3D**). In immunohistochemistry on cryosections, we showed that Pomt1 localizes in both longitudinal and junctional sarcoplasmic reticulum (SR), as previously described in mouse and humans (29), and that ryanodine receptor 1 (Ryr1) in the SR around the T tubules is greatly reduced as found in *patchytail,* the *dag1* mutant fish (**Fig.3E**) (20). The same loss of Ryr1 staining was also present at 10 dpf, when no other phenotypes were evident (**Suppl. Fig.1D**). Although milder than expected, these results show overall that loss of *pomt1* in the zebrafish leads to deficits in muscle function and structure.

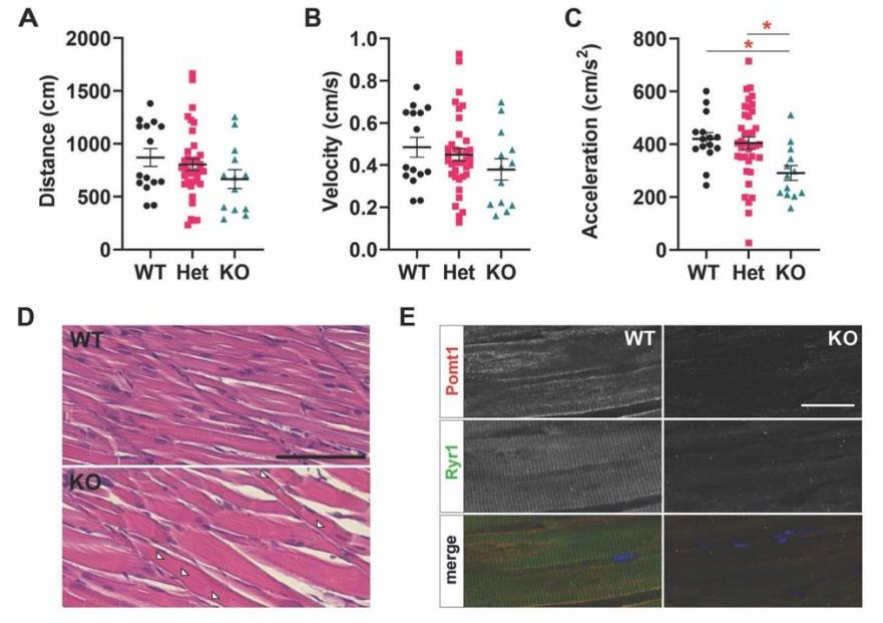

Figure 3. Muscle phenotypes in 30 dpf *pomt1* KO juvenile zebrafish. A-C. Automated tracking of motor activity showed only a trend for reduction in distance (**A**) and velocity (**B**), but significant reduction in acceleration (**C**) in KO animals compared to WT and Het. * p<0.05 **D.** Muscle histology in paraffin

sections stained with hematoxylin and eosin showed separated fibers of variable size and gaps in the myosepta (arrowheads). Scale bar: 50 μm. **E.** Muscle immunohistochemistry on cryosections showed loss of Pomt1 staining. Ryr1 from the junctional SR around T tubules is also absent in KO muscle. Scale bar: 20 μm.

pomt1 loss-of-function disrupts photoreceptor synapses

While the brain of 30 dpf *pomt1* KO fish showed no major structural abnormalities, a mutant for the glycosyltransferase *pomgnt1* showed photoreceptor degeneration between 2 and 6 months of age (22). While eye size in *pomt1* KOs was highly variable and only trended towards being smaller, it was proportional to body size (**Suppl. Fig.2A**). We chose to analyze the smaller *pomt1* KO fish that were likely to be more severely affected. Retinal thickness and photoreceptor layer thickness were reduced at 30 dpf and the photoreceptor layer was disproportionally thinner than the retina (**Suppl. Fig.2B**. Retina/photoreceptor ratio. WT n=6: 0.390±0.018, KO n=5: 0.297±0.027, p=0.015 *)**.** Through immunohistochemical analysis we noted several disruptions in the photoreceptor layer and in the outer plexiform layer (OPL) where photoreceptor pedicles form synapses with bipolar cells and horizontal cells to begin the transmission of light signals. Immunostaining with the red/green double cone maker arrestin3a (Arr3a) which also accumulates at the presynaptic pedicles of the photoreceptors (30) showed a disruption in the organization of terminals in the OPL with some terminals retracting among the photoreceptor nuclei (**Fig.4A**). Expression of Gnat2, a cone-specific α-transducin subunit necessary for the phototransduction cascade and color vision (31), showed reduced staining in the outer limiting membrane and in the photoreceptor outer segments (**Fig.4A**). In addition, the rod and green cone marker, zpr-3, which is predicted to bind outer segment opsins (32) also showed localized reduced staining, though rod outer segments appear present in autofluorescence (**Fig.4B**). OPL disorganization was evident in the Hoechst nuclear staining, where localized misalignments of photoreceptor nuclei were present, as well as smaller and misshapen horizontal cell nuclei (**Fig.4B**). These disruptions suggested a loss of photoreceptor-bipolar cell synapses. Discontinuities in the expression of presynaptic protein synaptophysin (Syp) were present wherever photoreceptor pedicles were lost (**Fig.4C**). Overall, our results were similar to the phenotypes in both *pomgnt1* KO zebrafish and *Pomt1* conditional removal in photoreceptors in mice where loss of dystroglycan glycosylation leads to disruptions at photoreceptor ribbon synapses and subsequent photoreceptor degeneration (12,22).

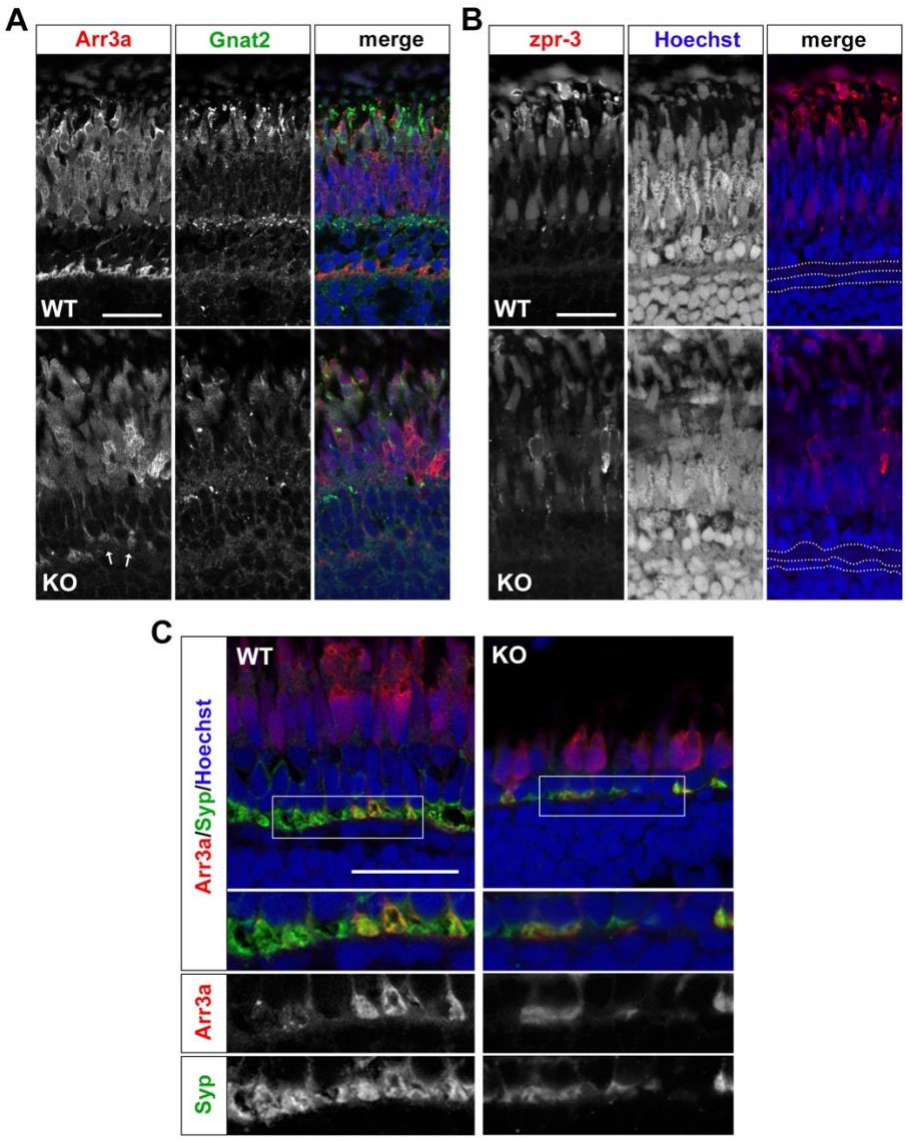

Figure 4. Photoreceptor synapses are disrupted in *pomt1* KO retinae. A. Red/green double cone marker arrestin 3a (Arr3a) shows both a disorganization in the outer segment and retraction of photoreceptors pedicles in the outer plexiform layer (OPL) (arrows). Cone-specific α-transducin (Gnat2) staining is also reduced and lost in the outer limiting membrane. Scale bar: 20 μm **B.** zpr-3 staining is reduced, but rods appear present in autofluorescence. Nuclear staining with Hoechst shows disorganization in the OPL and disruption in the nuclei of the horizontal cells below the OPL. OPL and horizontal cell nuclear layer are outlined by the white dotted lines. Scale bar: 20 μm **C.** Synaptophisin (Syp) staining is discontinuous and showing loss of synaptic contacts. The white boxes outline the inset where immunostaining for each antibody is shown below. Scale bar: 20 μm

More severe dystroglycanopathy phenotypes are present when pomt1 is removed from fertilized oocytes.

Even though muscle and eye phenotypes characteristic of dystroglycanopathies were present in the *pomt1* KO juveniles, they presented later than expected when compared to *dag1* zebrafish mutants (20). Not only are zebrafish notorious for being able to compensate for genetic mutations (33), but also display a fundamental difference from mammals in that a deposit of mRNA and proteins provided by the mother in the yolk sac supports early development of the externally fertilized egg (25). *pomt1* mRNA is highly expressed in the maternal deposit (19) and glycosylated α-DG is stable for several days in tissues (34). We hypothesized that the appearance of dystroglycanopathy phenotypes in *pomt1* KO fish was delayed due to residual Pomt1 function in the embryo provided by the Het mother.

Molecular investigation by western blot at 5 dpf indicated that *pomt1* KO larvae obtained from Het females (herein KO^{Het}) retained both the Pomt1 protein and substantial α-DG glycosylation (**Fig.5A**). We were able to support several KO^{Het} females to survive to breeding age by reducing stocking density and decreasing competition for food. This allowed us to investigate whether offspring from oocytes lacking *pomt1* would have more severe phenotypes. 5 dpf *pomt1* KO larvae obtained from KO female x Het male crosses (KO^{KO}) showed no residual Pomt1 expression or α-DG glycosylation (**Fig.5B**). As observed in the *dag1* mutant zebrafish (20), survival in *pomt1* KO^{KO} larvae decreased rapidly after 10 dpf (**Fig.5C**). In parallel, body size was significantly reduced starting at 10 dpf (Het: 4.39±0.05 mm, n=51; KO^{KO}: 3.97±0.05 mm, n=43, N=3 clutches. p<0.0001 ***) (**Fig.5D**). Interestingly, size disparities were variable at 20 dpf, the timepoint at which KO^{KO} fish started dying. Clutches where most KO^{KO} larvae had died showed no significant size differences (Het: 5.63±0.10 mm, n=63; KO^{KO}: 5.40±0.20 mm, n=12, N=3 clutches. p=0.366) (**Suppl. Fig.3A**), while a clutch with a 50/50 ratio of Hets and KO^{KO}s showed a significant size reduction (Het: 5.93±0.14 mm, N=1, n=12; KO^{KO}: 5.08±0.11, N=1, n=12. p<0.0001 ***) (**Fig. 5D, Suppl. Fig.3B**), again showing that the largest fish can survive better. By 30 dpf, the few surviving fish were smaller than the Het^{KO} siblings (Het: 7.17±0.14 mm, n=58; KO^{KO}: 6.22±0.20, n=8, N=3 clutches. p<0.0001 ***).

Locomotor activity was significantly impacted in pomt1 KO^{KO} larvae at 5 dpf with reductions in distance traveled, velocity and acceleration, showing that even if survival and size were not affected mobility was already severely impacted at an early age (Het n=57, KO^{KO} n=36, N=3 clutches. Distance: Het: 345.2±117.3 cm, KO^{KO}: 231.4±0.11, p<0.0001 ***; Velocity: Het: 0.19±0.06 cm/s, KO^{KO}: 0.13±0.04 cm/s, p<0.0001 ***; Acceleration: Het: 166.6±67.6 cm/s^2, KO^{KO}: 81.63±67.34 cm/s^2, p<0.0001 ***)(**Fig.6A-C**). Muscle integrity analysis using birefringence using polarized light to detect muscle fiber organization showed reduced intensity (**Fig.6D**). Immunohistochemistry on cryosections using

238 fluorescently stained phalloidin to outline actin in muscle fibers showed some modest discontinuities in
239 staining and revealed widenings in the myosepta as observed at 30 dpf in KO^{Het}s indicating the beginning
240 of muscle disease (**Fig.6E**).
241

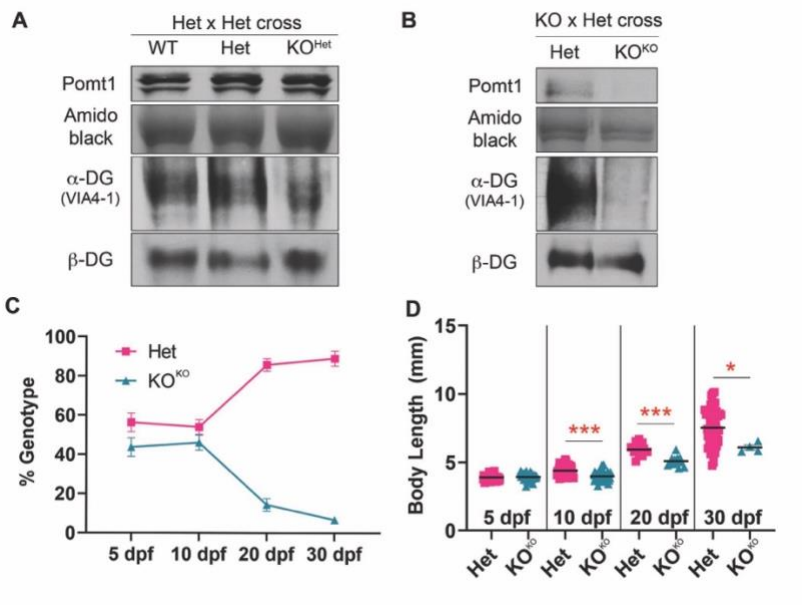

242

243 **Figure 5. Removal of maternal *pomt1* mRNA contribution from oocytes leads to earlier phenotypes in**
244 ***pomt1* KO^{KO} larvae. A.** Residual Pomt1 is present in 5 dpf KO^{Het} larvae derived from Het X Het crosses, as
245 is α-DG glycosylation. **B.** Both Pomt1 and α-DG glycosylation are absent at 5 dpf in KO^{KO} larvae obtained
246 from KO mothers crossed with Het fathers. **C.** Survival in *pomt1* KO^{KO} zebrafish is reduced starting at 10
247 dpf. **D.** Reduced body size is observed in KO^{KO} larvae and juveniles starting at 10 dpf. *** p<0.001, *
248 p<0.05
249

250 **Figure 6 (image on following page). *pomt1* KO^{KO} larvae show reduced mobility and muscle disease at 5**
251 **dpf. A-C.** A significant reduction in total distance traveled (**A.**), velocity (**B.**) and acceleration (**C.**) are
252 found in *pomt1* KO^{KO} larvae upon automated mobility analysis when compared to Het siblings. ***
253 p<0.001. **D.** Birefringence analysis showed patchy light diffraction through the KO^{KO} muscle showed
254 disorganized muscle tissue. Scale bar: 500 μm. **E.** Staining with fluorescently labeled phalloidin to
255 visualize actin in muscle fibers revealed some fiber disorganization, variable staining intensity, and
256 increased space between muscle segments in the myosepta (arrowheads) of KO^{KO} larvae. Scale bar: 100
257 μm

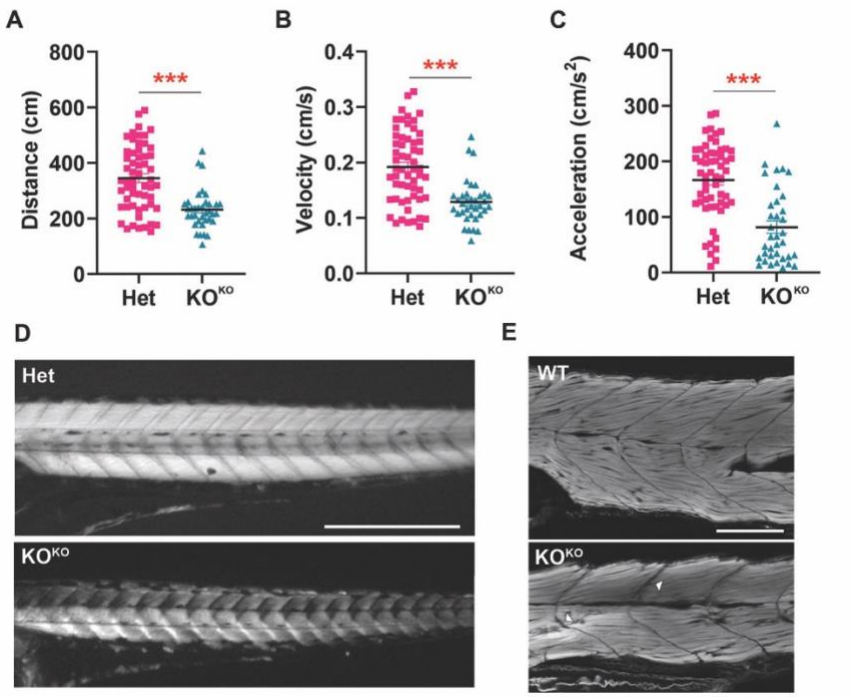

Retinal phenotypes observed at 30 dpf in KO^{Het} fish were present at 5 dpf in the KO^{KO} larvae. Arr3a staining in cone photoreceptors was patchy and nuclei were disorganized in the outer nuclear layer of photoreceptors (**Fig.7A**). Synaptic staining with Syp in the OPL was discontinuous, often extending into the outer nuclear layer indicating retraction of photoreceptor pedicles indicating an early loss of synapses between photoreceptors and bipolar cells (**Fig.7A**, **Suppl. Fig.4**). One major phenotype caused by loss of α-DG glycosylation in mice is the disruption of axonal tracts in the brain caused by loss of interaction with axon guidance cues (35,36). One example is the disruption in retinal ganglion cell sorting and fasciculation in the optic nerve which is controlled by binding to the midline crossing cue Slit2, an α-DG ligand (36,37). We did not see any deficits in axonal crossing and fasciculation in the optic chiasm of 30 dpf KO^{Het} fish (**Suppl. Fig.5**), but we wondered whether the maternal deposit of *pomt1* was sufficient to bypass this early developmental phenotype. When we analyzed the optic chiasm using the zn8 antibody that labels retinal ganglion cells and their axons, we noted substantial axonal defasciculation following axon crossing at the optic chiasm of KO^{KO} larvae reminiscent of phenotypes found following *slit2* knockout and knockdown in the fish (**Fig.7B**) (38). Thus, *pomt1* loss of function early in development in the zebrafish also recapitulates some of the central nervous system phenotypes found in higher vertebrates.

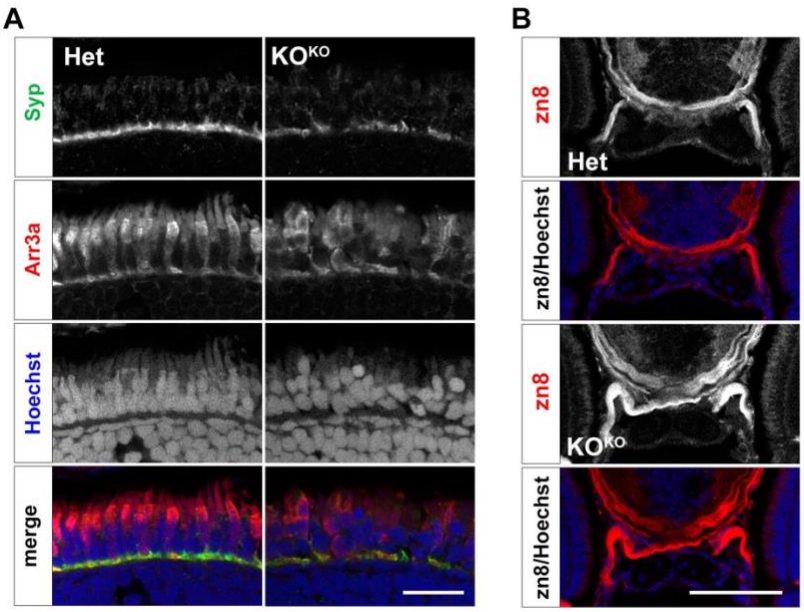

Figure 7. Retinal and axon guidance phenotypes are found at 5 dpf in *pomt1* KO^{KO} larvae. A. Discontinuities in synaptophysin (Syp) staining are found in the outer plexiform layer (OPL) of *pomt1* KO^{KO} retinae. Red/green double cone marker arrestin 3a (Arr3a) again shows disorganized outer segments and patchy staining and altered shape of photoreceptors pedicles. Nuclear staining with Hoechst shows disorganization disruption in the photoreceptor nuclei and in horizontal cell nuclei below the OPL. Scale bar: 20 μm. **B.** Visualization of the optic nerve using the zn8 antibody that labels retinal ganglion cell axons shows axon defasciculation after optic chiasm crossing. Scale bar: 50 μm.

Discussion

Here, we showed that *pomt1* KO zebrafish can be used to model dystroglycanopathy phenotypes in the muscle, eye, and brain with variable severity. For our initial analysis of this mutant strain we focused on phenotypes identified in other dystroglycanopathy models in fish and mouse. The phenotypes found in *pomt1* KO^{Het} obtained from heterozygous crosses were milder than those observed in the *dag1* loss of function fish (20) suggesting that compensation may be present. We found that this was due to high *pomt1* mRNA expression in the maternal deposit in the oocyte supporting α-DG glycosylation during the first week post fertilization. While we still found Pomt1 expression at 5 dpf in KO^{Het} larvae, the protein was largely absent from the muscle at 10 dpf. In parallel, *pomt1* mRNA levels that were consistently lower than WT at all other timepoints were increased at 10 dpf likely in response to loss of the maternal protein. Even if Pomt1 was lost by 10 days, studies in mouse muscle have shown that dystroglycan can remain for up to 20 days in tissues (39). We found that in *pomt1* KO^{Het} fish α-DG glycosylation was completely lost by

30 dpf when disease-related phenotypes in the muscle and retina began to emerge. KO^{Het} juveniles maintained at high stocking density started dying at 30 dpf with no survivors found past 70 days. We noted that *pomt1* KOs surviving the longest were the largest and showed the least severe phenotypes suggesting that impaired mobility and/or vision may prevent the smaller KOs from having access to food in the tank. Some KO fish could only be raised when stocking density was reduced to remove competition for food. These results indicate that even when the early developmental roles of α-DG are conserved, continued Pomt1 expression is necessary to maintain muscle function and retinal photoreceptors integrity.

By raising KO females, we were able to obtain oocytes completely devoid of *pomt1* mRNA to generate true developmental KOs where α-DG O-mannosylation is prevented from time of fertilization. *pomt1* KO^{KO}s closely resembled other dystroglycanopathy models in both zebrafish and mouse. As in the *dag1* mutant, *patchytail*, *pomt1* KO^{KO}s died within the first 2 weeks post fertilization. The muscle displayed abnormal birefringence, openings in the myotendenous junctions or myosepta between muscle segments, and loss of Ryr1 staining in the SR. These deficits led to substantial mobility phenotypes at 5 dpf. At the same time, we identified defects in photoreceptor synapses and optic nerve fasciculation in the KO^{KO} larvae reflecting loss of α-DG ligand binding necessary for synapse formation and axon guidance that had been previously described in *pomt1* conditional mouse models and *pomgnt1* mutant zebrafish (12,22).

α-DG can bind to a variety of proteins containing laminin-G domains (40) and several of its ligands have important roles in axon guidance and synapse formation in the brain and peripheral nervous system (35,37,41). Slits are involved in guiding axons in crossing the midline of the body and contribute to the formation of the optic chiasm where axons from each eye target brain regions on the opposite side (42). α-DG was shown to bind to the laminin-G domain of Slit2 to organize axonal crossing (37) and the phenotypes observed in the *pomt1* KO^{KO} larval optic chiasm are similar to the enlarged and disorganized axonal tract found in *slit2* KO zebrafish (43). Another α-DG ligand is pikachurin, a postsynaptic adhesion protein involved in the formation and maintenance of photoreceptor ribbon synapses (41,44). Ribbon synapses are highly specialized structures in the photoreceptor pedicles in the OPL mediating rapid transmission of visual signals to the dendrite tips of horizontal cells and bipolar cells. When the bond between α-DG and pikachurin is lost, the synapse comes apart and photoreceptors pedicles retract eventually leading to photoreceptor degeneration and loss of vision (12,41,44). Our findings in *pomt1* KO^{KO}s closely recapitulate phenotypes in a mutant mouse line where *Pomt1* is conditionally removed in photoreceptors (12). Additional analyses will be needed to determine whether synapses and laminar organization in other retinal layers are also affected as described in mouse models (45). Changes in

synaptophysin staining in the inner plexiform layer shown in our supplementary data suggest that this may be the case. Overall, early developmental phenotypes caused by loss of matriglycan binding in multiple tissues are present in the *pomt1* KO^{KO} supporting the need to further study of this model to determine the impact of these mutations in the brain and peripheral nervous system.

While *pomt1* KO^{KO} and the *dag1* ENU mutant are similar, their phenotypes are overall less severe than those observed the *fkrp* mutant line which in turn recapitulate morphant models for *fkrp* and other glycosyltransferases mutated in dystroglycanopathies (16,17,21,46). Morphants for *fkrp*, *pomgnt1* and *b3galnt2* larvae show early mortality, shorter body, smaller head and eyes and severe cardiac edema. On the other hand, *pomt1* morphants were less severe than other morphants showing milder morphological disruptions (19). Thus, we believe that KO^{KO} animals reflect complete loss of function of *pomt1* in the fish and can be studied as a valid model of dystroglycanopathy phenotypes in the muscle, eye, and brain. Our study stresses how maternal mRNA and protein contribution must be taken into consideration when generating dystroglycanopathy models since the long-lasting presence of glycosylated α-DG can mask developmental phenotypes in the embryo. At the same time, a later onset model where pathogenesis progresses more slowly like the *pomt1* KO^{Het} fish could still be used to study the involvement of α-DG glycosylation in maintenance of tissue function. Both versions of this zebrafish model could be used to investigate therapeutic interventions in multiple tissues at different stages and severity of disease.

Materials and Methods

Zebrafish Husbandry

All experiments and procedures were conducted according to institutional guidance and approved by the Rutgers University Institutional Animal Care and Use Committee. *pomt1* mutant line was a kind gift from James Dowling (Sick Kids, Toronto, Canada). These animals were generated from the Zebrafish Mutation Project (line: sa146678, ZFIN ID: ZDB-ALT-130411-3355) on an AB background (26). The breeding stocks were bred and housed in recirculating Tecniplast USA systems under a 14/10 h light/dark (LD) cycle at 28°C and fed twice daily. To produce embryos, male and female zebrafish were paired in the evening, and spawning occurred within 1 h of lights-on the following morning. Embryos were placed in 10 cm petri dishes with egg water containing methylene blue (5 x 10^{-5} % w/v) and raised under LD cycles at 28°C.

Genotyping

DNA from larval tails and juvenile and adult tail fins was extracted using the Extract-N-Amp Tissue PCR Kit (Millipore Sigma). After verifying SNP location with Sanger sequencing at Azenta Life Sciences, genotype was determined using a Custom TaqMan SNP Genotyping Assay (Assay ID: ANRWEV2, Thermo Fisher).

Quantitative Real-Time PCR (qPCR) Gene Expression Analysis

Total RNA was isolated from embryo composite samples or adult tissue using ReliaPrep RNA Tissue Miniprep System (Promega). Reverse transcription was performed on RNA to produce cDNA for RT-PCR using an iScript Reverse Transcription Supermix (Bio-Rad) using a Bio-Rad T100 Thermal Cycler. RT-PCR reactions were performed in triplicate using PowerUp SYBR Green Master Mix (Thermo Fisher). cDNA amplification was performed for 40 cycles on a QuantStudio 3 (Applied Biosystems) and recorded with QuantStudio Design and Analysis Software. Analysis was conducted as $\Delta\Delta$CT using *elf1-alpha* or *rpl13* as an endogenous control. All primer sequences are available upon request.

Wheat Germ Agglutinin Enrichment and Western Blot Analysis

Total zebrafish protein was extracted from composite samples (5 dpf; N=60 and 30 dpf; N=3) using lysis buffer (50 mM Tris pH 8, 100 mM NaCl, 1 mM PMSF, 1 mM Na Orthovanadate, 1% Triton-X 100) containing protease inhibitor cocktail (Millipore Sigma), and 3 rounds of hand homogenization and vortexing. Samples were then sonicated in a Bransonic B200 Ultrasonic Cleaner (Millipore Sigma) 3 times for 5 minutes. Next samples were spun down at 4°C for 20 minutes at 15,000 xg. The supernatant was collected from the samples and sonicated once for 5 minutes. Total protein concentration was determined using a BCA Protein Assay kit (G-Biosciences) and subsequently treated with DNase I (New England Biolabs). 400-500 μg of protein was then added to 50 μl of Wheat Germ Agglutinin (WGA) agarose bound beads (Vector Laboratories) filled to a volume of 300 μl with Lectin Binding Buffer (20 mM Tris pH 8, 1 mM $MnCl_2$ and 1 mM $CaCl_2$) in a 1.5 ml tube and rocked overnight at 4°C. Samples were centrifuged at 15,000 xg for 2 minutes and the supernatant was collected. Volumes of supernatant containing 60 μg of protein were set aside for detection of Pomt1. Glycoproteins were eluted by boiling at 100°C for 10 minutes using 4x Laemmli sample buffer (Bio-Rad). Proteins were separated using a 4-12% Bis-Tris Protein SDS-PAGE Gel (Life Technologies). Samples were transferred to a nitrocellulose membrane (Thermo Fisher) and stained with 0.1% naphthol blue black (amido black) (Millipore Sigma) to detect protein transfer and for total protein quantification. The membranes were blocked for 1 hour with 5% milk in Tris-Buffered Saline with 0.1% Tween (TBST) and subsequently probed with 1:100 anti-α-

Dystroglycan antibody, clone VIA4-1 (05-298, Millipore Sigma) and 1:1,000 anti-β-Dystroglycan antibody (ab62373, Abcam) or anti-POMT1 (A10281, ABclonal) overnight at 4°C. Then probed with 1:3,000 peroxidase AffiniPure donkey anti-mouse IgG and 1:20,000 peroxidase AffiniPure donkey anti-rabbit IgG (Jackson ImmunoResearch). After washing with TBST, the blots were developed using chemiluminescence Pierce ECL Western Blotting Substrate on CL-XPosure™ Film (Thermo Fisher).

Morphological Analysis

Larvae and juvenile zebrafish were anesthetized in 0.016% w/v tricaine methane sulfonate (Tricaine, MS-222) and immobilized in 5% methyl cellulose for imaging with a M165 FC stereo microscope and LAS Software V4.21 (Leica Microsystems). Total body length measurements and eye area were quantified using Fiji/ImageJ software (47). Retinal and photoreceptor layer thickness were measured on cryosections prepared as described below and stained with Hoechst 33342 (1:10,000, Thermo Fisher) also using Fiji/ImageJ.

Automated Mobility Tracking

Automated mobility assays were conducted by randomizing 5, 20, and 30 dpf zebrafish into sterile 96 and 24-well plates filled with 200 µl and 2 ml of system water, respectively. Fish were then habituated in the DanioVision™ Observation Chamber (Noldus Information Technology, Wageningen) for 30 minutes at a controlled temperature of 28°C. Locomotor activity was tracked for 30 minutes using EthoVision® XT video tracking software. A minimum of three unique breeding sets were used to compile results at each timepoint.

Fluorescent Immunohistochemisty

Zebrafish larvae at 5 dpf were euthanized with tricaine and a small portion of the tail was cut to use for genotyping. The remaining fish body was fixed in 4% paraformaldehyde overnight at 4°C. Larvae were washed three times in 1x PBS, then cryoprotected in 15% sucrose with 0.025% sodium azide followed by 30% sucrose with 0.025% sodium azide. Larvae were embedded in Tissue Freeze Medium (TFM) (General Data Healthcare) and frozen in 2-methyl butane with dry ice. Juvenile fish processing required the addition of a decalcification step in Cal-Ex (Fisher Scientific) following fixation for 1 hour and 15 minutes rocking at 4°C. Cryosections were performed using a Leica CM1850 UV Cryostat (Leica Microsystems) at 10 µm for 5 dpf, 12 µm for 10 dpf, and 16 µm for 30 dpf. Primary antibodies were applied overnight at 4°C in 1% normal goat serum (NGS) with 0.1% Triton following a blocking step with 10% NGS. Secondary

immunostaining was applied for 1 hour. The following antibodies were used: primary - POMT1 (A10281, 1:100, ABclonal), Gnat2 (A10352, 1:200, ABclonal), Synaptophysin (ab32127, 1:100, Abcam), Ryr1 (MA3-925, 1:100, Thermo Fisher), zpr-1 (Arr3a) (zpr-1, 1:200, ZIRC), zpr-3 (zpr-3, 1:200, ZIRC), zn-8 (zn-8-s, 1:100, DSHB); secondary - goat anti-mouse IgG Alexa Fluor 568, goat anti-rabbit Alexa Fluor 488 or goat anti-rabbit Alexa Fluor 568 (all from Thermo Fisher). Slides were washed twice in 1x PBS at room temperature and Hoechst 33342 (1:10,000, Thermo Fisher) was applied in 1x PBS for 5 minutes. F-actin/phalloidin staining was performed using Acti-Stain™ 555 (Cytoskeleton Inc.) at a concentration of 100 nM in 1x PBS and kept in the dark for 30 minutes at room temperature. Slides were then washed three times in 1x PBS for 2 minutes. Slides were coverslipped using ProLong™ Gold Antifade Mountant (Thermo Fisher). Images were taken using a Zeiss LSM800 confocal microscope and Zeiss Zen imaging software.

Paraffin Sectioning and Hematoxylin & Eosin Staining

Paraffin sectioning was performed by the Rutgers Cancer Institute of New Jersey Biospecimen Repository and Histopathology Service Shared Resource. Decalcified juvenile fish were placed in 70% Ethanol. Specimens were then dehydrated through a step protocol using ethanol and xylene and embedded in paraffin using a Sakura Tissue-Tek VIP6 AI tissue processor and a Sakura Tissue-Tek TEC 6 tissue embedder. Each mold was sectioned on a Leica Reichert-Jung BioCut 2030 rotary microtome at 4 μm. Slides were then deparaffinized and stained with hematoxylin and eosin using a Sakura Tissue-Tek DRS 2000 slide stainer.

Statistical Analysis

Data represent the mean ± SEM or are presented as scatter plots with the mean. All statistical analyses were performed using GraphPad Prism v.8.20 (GraphPad, San Diego, CA). To compare *in vivo* data for two groups, individual means were compared using the MannWhitney U test and Welch's t test. When comparing more than three groups, normality was assessed using the Shapiro-Wilk test, then a two-way ANOVA with Tukey's post hoc test was used for normally distributed samples or a Kruskal-Wallis test with Dunn's post-hoc test was used for non-normally distributed samples. All statistical analyses were two-sided tests, and p values of ≤ 0.05 were considered statistically significant.

Acknowledgements

The authors would like to thank Dr. James Dowling (Sick Kids, Toronto, ON, Canada) for donating the sa146678 mutant line. We also thank Drs. John Dowling (Harvard University) and Ellen Townes-Anderson

(New Jersey Medical School) for helpful discussion on zebrafish photoreceptor phenotypes and retinal degeneration, and Dr. Matthew Alexander (University of Alabama, Birmingham) for discussion on the muscle phenotypes. We are particularly grateful to Kathleen Flaherty at the Rutgers Zebrafish Facility with assistance in the maintenance of the zebrafish colony and Lucyann Franciosa and Kelly Watkinswalton at the Rutgers Cancer Institute of New Jersey Biospecimen Repository and Histopathology Service Shared Resource for paraffin sectioning. The zn-8 developed by University of Oregon, Department of Neuroscience was obtained from the Developmental Studies Hybridoma Bank, created by the NICHD of the NIH and maintained at The University of Iowa, Department of Biology, Iowa City, IA 52242.

Conflict of Interest Statement. The authors declare no competing interests.

Funding

This work was funded by National Institute of Neurological Disorders and Stroke (R01NS109149 to M.C.M) and the Robert Wood Johnson Foundation (#74260 to M.C.M). B.F.K was supported by grant T32NS115700 from National Institute of Neurological Disorders and Stroke. Histopathology services in support of the research project were provided by the Rutgers Cancer Institute of New Jersey Biospecimen Repository and Histopathology Service Shared Resource supported in part with funding from National Cancer Institute (NCI-CCSG P30CA072720-5919).

Abbreviations

α-DS - α-dystroglycan
CMD - congenital muscular dystrophy
dpf – day post fertilization
ECM - extracellular matrix
Het – heterozygous
KO – knock-out
LGMD - limb-girdle muscular dystrophy
MO - morpholino oligonucleotides
OPL - outer plexiform layer
WT – wild type
WWS – Walker Warburg Syndrome

References

1. Bönnemann, C.G., Wang, C.H., Quijano-Roy, S., Deconinck, N., Bertini, E., Ferreiro, A., Muntoni, F., Sewry, C., Béroud, C., Mathews, K.D., *et al.* (2014) Diagnostic approach to the congenital muscular dystrophies. Neuromuscular disorders : NMD, Vol. 24, pp. 289–311.

2. Kanagawa, M. (2021) Dystroglycanopathy: From Elucidation of Molecular and Pathological Mechanisms to Development of Treatment Methods. *Int J Mol Sci*, 22, 13162.

3. Yoshida-Moriguchi, T. and Campbell, K.P. (2015) Matriglycan: a novel polysaccharide that links dystroglycan to the basement membrane. *Glycobiology*, 25, 702–713.

4. Brancaccio, A. (2019) A molecular overview of the primary dystroglycanopathies. *J Cell Mol Med*, 23, 3058–3062.

5. Kim, D.-S., Hayashi, Y.K., Matsumoto, H., Ogawa, M., Noguchi, S., Murakami, N., Sakuta, R., Mochizuki, M., Michele, D.E., Campbell, K.P., *et al.* (2004) POMT1 mutation results in defective glycosylation and loss of laminin-binding activity in &agr;-DG. *Neurology*, 62, 1009–1011.

6. Graziano, A., Bianco, F., D'Amico, A., Moroni, I., Messina, S., Bruno, C., Pegoraro, E., Mora, M., Astrea, G., Magri, F., *et al.* (2015) Prevalence of congenital muscular dystrophy in Italy: a population study. *Neurology*, 84, 904–911.

7. Sframeli, M., Sarkozy, A., Bertoli, M., Astrea, G., Hudson, J., Scoto, M., Mein, R., Yau, M., Phadke, R., Feng, L., *et al.* (2017) Congenital muscular dystrophies in the UK population: Clinical and molecular spectrum of a large cohort diagnosed over a 12-year period. *Neuromuscular Disord*, 27, 793–803.

8. Song, D., Dai, Y., Chen, X., Fu, X., Chang, X., Wang, N., Zhang, C., Yan, C., Zheng, H., Wu, L., *et al.* (2020) Genetic Variations and Clinical Spectrum of Dystroglycanopathy in a Large Cohort of Chinese Patients. *Clin Genet*.

9. Willer, T., Prados, B., Falcón-Pérez, J.M., Renner-Müller, I., Przemeck, G.K.H., Lommel, M., Coloma, A., Valero, M.C., Angelis, M.H. de, Tanner, W., *et al.* (2004) Targeted disruption of the Walker-Warburg syndrome gene Pomt1 in mouse results in embryonic lethality. *Proceedings of the National Academy of Sciences of the United States of America*, 101, 14126–14131.

10. Cohn, R.D., Henry, M.D., Michele, D.E., Barresi, R., Saito, F., Moore, S.A., Flanagan, J.D., Skwarchuk, M.W., Robbins, M.E., Mendell, J.R., *et al.* (2002) Disruption of DAG1 in differentiated skeletal muscle reveals a role for dystroglycan in muscle regeneration. *Cell*, 110, 639–648.

11. Satz, J.S., Barresi, R., Durbeej, M., Willer, T., Turner, A., Moore, S.A. and Campbell, K.P. (2008) Brain and eye malformations resembling Walker-Warburg syndrome are recapitulated in mice by dystroglycan deletion in the epiblast. *Journal of Neuroscience*, 28, 10567–10575.

12. Rubio-Fernández, M., Uribe, M.L., Vicente-Tejedor, J., Germain, F., Susín-Lara, C., Quereda, C., Montoliu, L., Villa, P. de la, Martín-Nieto, J. and Cruces, J. (2018) Impairment of photoreceptor ribbon

522 synapses in a novel Pomt1 conditional knockout mouse model of dystroglycanopathy. *Sci Rep-uk*, 8,
523 8543.

524 13. Li, M., Hromowyk, K.J., Amacher, S.L. and Currie, P.D. (2017) Chapter 14 Muscular dystrophy
525 modeling in zebrafish. *Methods Cell Biol*, 138, 347–380.

526 14. Widrick, J.J., Kawahara, G., Alexander, M.S., Beggs, A.H. and Kunkel, L.M. (2019) Discovery of Novel
527 Therapeutics for Muscular Dystrophies using Zebrafish Phenotypic Screens. *Journal of neuromuscular*
528 *diseases*, 6, 271–287.

529 15. Carss, K.J., Stevens, E., Foley, A.R., Cirak, S., Riemersma, M., Torelli, S., Hoischen, A., Willer, T.,
530 Scherpenzeel, M. van, Moore, S.A., *et al.* (2013) Mutations in GDP-Mannose Pyrophosphorylase B Cause
531 Congenital and Limb-Girdle Muscular Dystrophies Associated with Hypoglycosylation of α-Dystroglycan.
532 *American journal of human genetics*.

533 16. Stevens, E., Carss, K.J., Cirak, S., Foley, A.R., Torelli, S., Willer, T., Tambunan, D.E., Yau, S., Brodd, L.,
534 Sewry, C.A., *et al.* (2013) Mutations in B3GALNT2 Cause Congenital Muscular Dystrophy and
535 Hypoglycosylation of α-Dystroglycan. *American journal of human genetics*.

536 17. Manzini, M.C., Tambunan, D.E., Hill, R.S., Yu, T.W., Maynard, T.M., Heinzen, E.L., Shianna, K.V.,
537 Stevens, C.R., Partlow, J.N., Barry, B.J., *et al.* (2012) Exome sequencing and functional validation in
538 zebrafish identify GTDC2 mutations as a cause of Walker-Warburg syndrome. *American journal of*
539 *human genetics*, 91, 541–547.

540 18. Costanzo, S.D., Balasubramanian, A., Pond, H.L., Rozkalne, A., Pantaleoni, C., Saredi, S., Gupta, V.A.,
541 Sunu, C.M., Yu, T.W., Kang, P.B., *et al.* (2014) POMK mutations disrupt muscle development leading to a
542 spectrum of neuromuscular presentations. *Human Molecular Genetics*.

543 19. Avsar-Ban, E., Ishikawa, H., Manya, H., Watanabe, M., Akiyama, S., Miyake, H., Endo, T. and Tamaru,
544 Y. (2010) Protein O-mannosylation is necessary for normal embryonic development in zebrafish.
545 *Glycobiology*, 20, 1089–1102.

546 20. Gupta, V., Kawahara, G., Gundry, S.R., Chen, A.T., Lencer, W.I., Zhou, Y., Zon, L.I., Kunkel, L.M. and
547 Beggs, A.H. (2011) The zebrafish dag1 mutant: a novel genetic model for dystroglycanopathies. *Human*
548 *Molecular Genetics*, 20, 1712–1725.

549 21. Serafini, P.R., Feyder, M.J., Hightower, R.M., Garcia-Perez, D., Vieira, N.M., Lek, A., Gibbs, D.E.,
550 Moukha-Chafiq, O., Augelli-Szafran, C.E., Kawahara, G., *et al.* (2018) A limb-girdle muscular dystrophy 2I
551 model of muscular dystrophy identifies corrective drug compounds for dystroglycanopathies. *JCI insight*,
552 3, 199.

553 22. Liu, Y., Yu, M., Shang, X., Nguyen, M.H.H., Balakrishnan, S., Sager, R. and Hu, H. (2020) Eyes shut
554 homolog (EYS) interacts with matriglycan of O-mannosyl glycans whose deficiency results in EYS
555 mislocalization and degeneration of photoreceptors. *Sci Rep-uk*, 10, 7795.

556 23. Diesen, C., Saarinen, A., Pihko, H., Rosenlew, C., Cormand, B., Dobyns, W.B., Dieguez, J., Valanne, L.,
557 Joensuu, T. and Lehesjoki, A.-E. (2004) POMGnT1 mutation and phenotypic spectrum in muscle-eye-
558 brain disease. *Journal of Medical Genetics*, 41, e115.

559 24. Xu, M., Yamada, T., Sun, Z., Eblimit, A., Lopez, I., Wang, F., Manya, H., Xu, S., Zhao, L., Li, Y., *et al.*
560 (2016) Mutations in POMGNT1 cause non-syndromic retinitis pigmentosa. *Hum Mol Genet*, 25, 1479–
561 1488.

562 25. Abrams, E.W. and Mullins, M.C. (2009) Early zebrafish development: It's in the maternal genes. *Curr*
563 *Opin Genet Dev*, 19, 396–403.

564 26. Kettleborough, R.N.W., Busch-Nentwich, E.M., Harvey, S.A., Dooley, C.M., Bruijn, E. de, Eeden, F.
565 van, Sealy, I., White, R.J., Herd, C., Nijman, I.J., *et al.* (2013) A systematic genome-wide analysis of
566 zebrafish protein-coding gene function. *Nature*, 496, 494–497.

567 27. Manzini, M.C., Gleason, D., Chang, B.S., Hill, R.S., Barry, B.J., Partlow, J.N., Poduri, A., Currier, S.,
568 Galvin-Parton, P., Shapiro, L.R., *et al.* (2008) Ethnically diverse causes of Walker-Warburg syndrome
569 (WWS): FCMD mutations are a more common cause of WWS outside of the Middle East. *Human*
570 *Mutation*, 29, E231-41.

571 28. Godfrey, C., Clement, E., Mein, R., Brockington, M., Smith, J., Talim, B., Straub, V., Robb, S.,
572 Quinlivan, R., Feng, L., *et al.* (2007) Refining genotype phenotype correlations in muscular dystrophies
573 with defective glycosylation of dystroglycan. *Brain : a journal of neurology*, 130, 2725–2735.

574 29. Akasaka-Manya, K., Manya, H., Nakajima, A., Kawakita, M. and Endo, T. (2006) Physical and
575 functional association of human protein O-mannosyltransferases 1 and 2. *The Journal of biological*
576 *chemistry*, 281, 19339–19345.

577 30. Renninger, S.L., Gesemann, M. and Neuhauss, S.C.F. (2011) Cone arrestin confers cone vision of high
578 temporal resolution in zebrafish larvae. *Eur J Neurosci*, 33, 658–667.

579 31. Kohl, S., Baumann, B., Rosenberg, T., Kellner, U., Lorenz, B., Vadalà, M., Jacobson, S.G. and
580 Wissinger, B. (2002) Mutations in the Cone Photoreceptor G-Protein α-Subunit Gene GNAT2 in Patients
581 with Achromatopsia. *Am J Hum Genetics*, 71, 422–425.

582 32. Gao, P., Qin, Y., Qu, Z., Huang, Y., Liu, X., Li, J., Liu, F. and Liu, M. (2022) The Zpr-3 antibody
583 recognizes the 320-354 region of Rho and labels both rods and green cones in zebrafish. *Biorxiv*,
584 2022.02.21.481375.

585 33. El-Brolosy, M.A., Kontarakis, Z., Rossi, A., Kuenne, C., Günther, S., Fukuda, N., Kikhi, K., Boezio,
586 G.L.M., Takacs, C.M., Lai, S.-L., *et al.* (2019) Genetic compensation triggered by mutant mRNA
587 degradation. *Nature*, 568, 193–197.

588 34. Novak, J.S., Spathis, R., Dang, U.J., Fiorillo, A.A., Hindupur, R., Tully, C.B., Mázala, D.A.G., Canessa, E.,
589 Brown, K.J., Partridge, T.A., *et al.* (2021) Interrogation of Dystrophin and Dystroglycan Complex Protein
590 Turnover After Exon Skipping Therapy. *J Neuromuscul Dis*, 8, S383–S402.

591 35. Lindenmaier, L.B., Parmentier, N., Guo, C., Tissir, F. and Wright, K.M. (2019) Dystroglycan is a scaffold
592 for extracellular axon guidance decisions. *eLife*, 8, 239.

593 36. Clements, R. and Wright, K.M. (2018) Retinal ganglion cell axon sorting at the optic chiasm requires
594 dystroglycan. *Dev Biol*, 442, 210–219.

595 37. Wright, K.M., Lyon, K.A., Leung, H., Leahy, D.J., Ma, L. and Ginty, D.D. (2012) Dystroglycan organizes
596 axon guidance cue localization and axonal pathfinding. *Neuron*, 76, 931–944.

597 38. Davison, C. and Zolessi, F.R. (2021) Slit2 is necessary for optic axon organization in the zebrafish
598 ventral midline. *Cells Dev*, 166, 203677.

599 39. Novak, J.S., Spathis, R., Dang, U.J., Fiorillo, A.A., Hindupur, R., Tully, C.B., Mázala, D.A.G., Canessa, E.,
600 Brown, K.J., Partridge, T.A., *et al.* (2021) Interrogation of Dystrophin and Dystroglycan Complex Protein
601 Turnover After Exon Skipping Therapy. *J Neuromuscul Dis*, 8, S383–S402.

602 40. Sheikh, M.O., Capicciotti, C.J., Liu, L., Praissman, J., Ding, D., Mead, D.G., Brindley, M.A., Willer, T.,
603 Campbell, K.P., Moremen, K.W., *et al.* (2022) Cell surface glycan engineering reveals that matriglycan
604 alone can recapitulate dystroglycan binding and function. *Nat Commun*, 13, 3617.

605 41. Sato, S., Omori, Y., Katoh, K., Kondo, M., Kanagawa, M., Miyata, K., Funabiki, K., Koyasu, T., Kajimura,
606 N., Miyoshi, T., *et al.* (2008) Pikachurin, a dystroglycan ligand, is essential for photoreceptor ribbon
607 synapse formation. *Nature Neuroscience*, 11, 923–931.

608 42. Plump, A.S., Erskine, L., Sabatier, C., Brose, K., Epstein, C.J., Goodman, C.S., Mason, C.A. and Tessier-
609 Lavigne, M. (2002) Slit1 and Slit2 cooperate to prevent premature midline crossing of retinal axons in
610 the mouse visual system. *Neuron*, 33, 219–232.

611 43. Davison, C. and Zolessi, F.R. (2021) Slit2 is necessary for optic axon organization in the zebrafish
612 ventral midline. *Cells Dev*, 166, 203677.

613 44. Omori, Y., Araki, F., Chaya, T., Kajimura, N., Irie, S., Terada, K., Muranishi, Y., Tsujii, T., Ueno, S.,
614 Koyasu, T., *et al.* (2012) Presynaptic Dystroglycan-Pikachurin Complex Regulates the Proper Synaptic
615 Connection between Retinal Photoreceptor and Bipolar Cells. *J Neurosci*, 32, 6126–6137.

616 45. Clements, R., Turk, R., Campbell, K.P. and Wright, K.M. (2017) Dystroglycan Maintains Inner Limiting
617 Membrane Integrity to Coordinate Retinal Development. *Journal of Neuroscience*, 37, 8559–8574.

618 46. Kawahara, G., Gasperini, M.J., Myers, J.A., Widrick, J.J., Eran, A., Serafini, P.R., Alexander, M.S.,
619 Pletcher, M.T., Morris, C.A. and Kunkel, L.M. (2014) Dystrophic muscle improvement in zebrafish via
620 increased heme oxygenase signaling. *Human Molecular Genetics*, 23, 1869–1878.

621 47. Schindelin, J., Arg, I., Arganda-Carreras, I., a-Carreras, Frise, E., Kaynig, V., Longair, M., Pietzsch, T.,
622 Preibisch, S., Rueden, C., *et al.* (2012) Fiji: an open-source platform for biological-image analysis. 9, 676–
623 82.

624